

Passivation of MBE grown InGaSb/InAs superlattice photodiodes

Cory J. Hill, Sam S. Keo, Jason. M. Mumolo, Sarath. D. Gunapala
Jet Propulsion Laboratory, 4800 Oak Grove Dr., Pasadena, CA USA 91109

ABSTRACT

We have performed wet chemical passivation tests on InGaSb/InAs superlattice photodiode structures grown by molecular beam epitaxy. The details of the devices growth and characterization as well as the results of chemical passivation involving RuCl_3 and H_2SO_4 with SiO_2 dielectric depositions are presented.

Keywords: Molecular beam epitaxy, superlattices, infrared detectors, infrared photodiodes, chemical passivation

1. INTRODUCTION

The closely lattice-match material system of InAs, GaSb, and AlSb, commonly referred to as the 6.1\AA material system, has emerged as a fertile ground for the development of new solid-state devices. The flexibility of the system in simultaneously permitting type-I, type-II staggered, and type-II broken-gap band alignments has been the basis for many novel, high-performance heterostructure devices in recent years, including the GaInSb/InAs type-II strained layer superlattice infrared detectors proposed by Smith and Mailhot¹ in 1987. The type-II superlattice design promises optical properties comparable to HgCdTe, better uniformity, reduced tunneling currents, suppressed Auger recombination, and normal incidence operation^{2,3}. In 1990, Chow and co-workers first reported Ga $_{1-x}$ In $_x$ Sb/InAs superlattice materials with high structural quality, LWIR photoresponse, and LWIR photoluminescence⁴. More recently, in 1997 researchers from Fraunhofer Institute demonstrated good detectivity (approaching HgCdTe, $8\text{-}\mu\text{m}$ cutoff, 77K) on individual devices⁵.

As illustrated in Fig.1, the band-gap of a type-II superlattice (SL) is determined by the energy separation between the first conduction miniband and the top-most heavy-hole miniband, rather than the band-gap of a bulk material. Hence, the SL structure can, in principle, be tailored by adjusting constituent layer thicknesses and compositions to cover a wide wavelength range for infrared detection.

In the type-II SL, heavy-holes are largely confined to the GaInSb layers and electrons are primarily confined to the InAs layers. However, because of the relatively low electron mass in InAs, the electron wavefunctions extend considerably beyond the interfaces and have significant overlap with heavy-hole wavefunctions. Hence, significant absorption is possible at the minigap energy (shown in Fig. 1 with the vertical arrow) which is tunable by changing layer thickness. It is also possible to obtain large optical absorption coefficients at cutoff wavelengths as long as $\sim 20\text{ }\mu\text{m}$ by taking advantage of internal lattice-mismatch-induced strains in the InAs/GaInSb SLs². Additionally, since the gap of each constituent bulk material is larger than the effective direct gap of the superlattice, dark currents are suppressed in comparison with their values in similar cutoff-wavelength bulk ternary alloys. Another benefit of this structure for detector applications is that normal incidence absorption is permitted by selection rules, obviating the need for grating structures or corrugations that are needed in alternative quantum-well infrared photodetectors (QWIPs)⁶. Finally, Auger transition rates, which place intrinsic limits on the performance of such detectors and severely impact the lifetimes found in the bulk, narrow-gap detectors, can be reduced by judicious choices for the structure's geometry and strain profile⁷.

Despite these advantages, there are still several challenges confronting the application of type-II superlattices as narrow-gap photodiodes, with the largest being the growth of thick, high quality strained layer superlattices and achieving an effective reduction of surface leakage currents and band-to-band as well as defect-assisted tunneling currents. Recent experimental results on such structures have shown real promise. For example, Fuchs and co-workers from the Fraunhofer Institute have demonstrated type-II InAs/GaInSb photodiodes having cutoff wavelengths ranging from 7.5 to $12\text{ }\mu\text{m}$ with performance characteristics similar to those obtained from HgCdTe-based diodes and argued that improvements in material and device quality would significantly enhance device performance⁵.

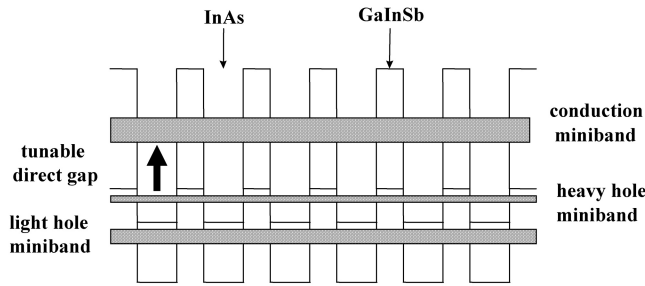


Figure 1. Schematic of the direct bandgap arising from the conduction and valence minibands in the GaInSb/InAs type-II superlattices.

2. DEVICE GROWTH

Superlattice photodiodes were grown in a Veeco Applied-Epi Gen III molecular beam epitaxy chamber equipped with valved cracking sources for the group V Sb₂ and As₂ fluxes, as well as dual In sources for independently varying the growth rates of GaInSb and InAs. Unintentionally doped p-type GaSb (100) substrates were placed in custom pyrolytic boron nitride holders with sapphire backing plates during growth. The device recipe is similar to that used by Fuchs⁵, consisting of a 0.5μm Be-doped GaSb buffer layer, followed by a p-i-n superlattice 30ÅGa_{0.8}In_{0.2}Sb/36ÅInAs with the first 88 periods Be doped in the GaInSb layers, 15 undoped periods, and the final 50 periods doped with Si in the InAs layers. The device is capped with a thin (200 to 300Å) layer of n-type InAs.

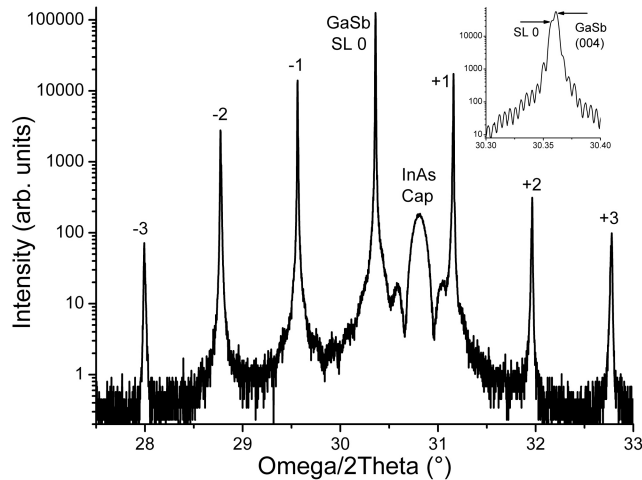


Figure 2. XRD scan of the superlattice diode near the GaSb (004) reflection. (Inset) Close-up of the substrate and zero-order superlattice peaks.

Fig. 2 shows a typical X-ray diffraction scan of the 30ÅGa_{0.8}In_{0.2}Sb/36ÅInAs device structure near the 004 reflection of the GaSb substrate. The overall periodicity of the structure as measured by the fringe spacing of the superlattice peaks is 64.4 Å, in good agreement with the recipe. The high structural quality of the epilayers is evidenced by the multiple sharp satellite peaks as well as the Pendellosung fringes from the thin InAs cap layer. The cross-sectional transmission

electron microscopy (TEM) image of the device in Fig. 3 shows no structural defects related to interface dislocations or strain relaxation during the growth of the superlattice layer.

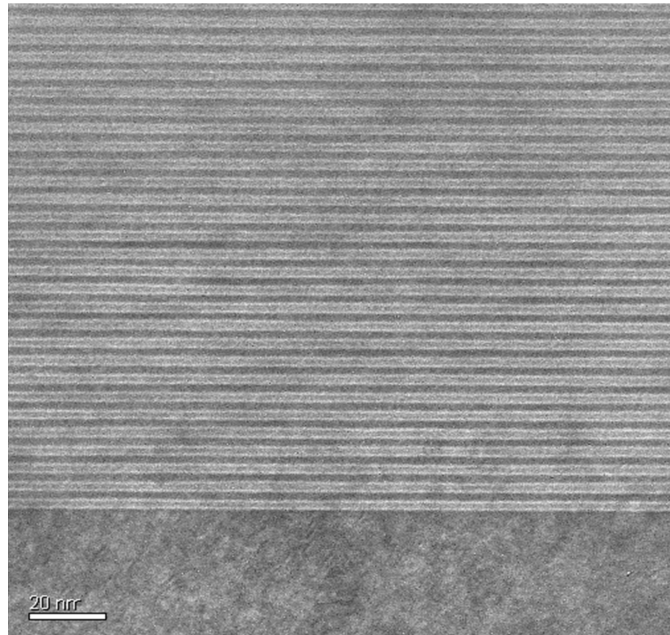


Figure 3. Cross-sectional TEM image of the InGaSb/InAs superlattice on the GaSb buffer layer.

Fig. 4 shows an atomic force microscope (AFM) scan of the surface of the epitaxial structure. The surface is very smooth, and typically no large defects are visible on a $50 \times 50 \mu\text{m}$ scan of the wafer surface. However, a high density of extremely shallow defects is apparent in the device growths. These defects are only visible with the AFM, as they are one the order of a few nm in height. Optical microscopy of the wafer surface reveals a density of roughly $200/\text{cm}^2$ of micron or larger sized defects. This density of large defects is entirely within the acceptable range for this type of epitaxial growth, and does not preclude the material from being suitable for focal plane array applications.

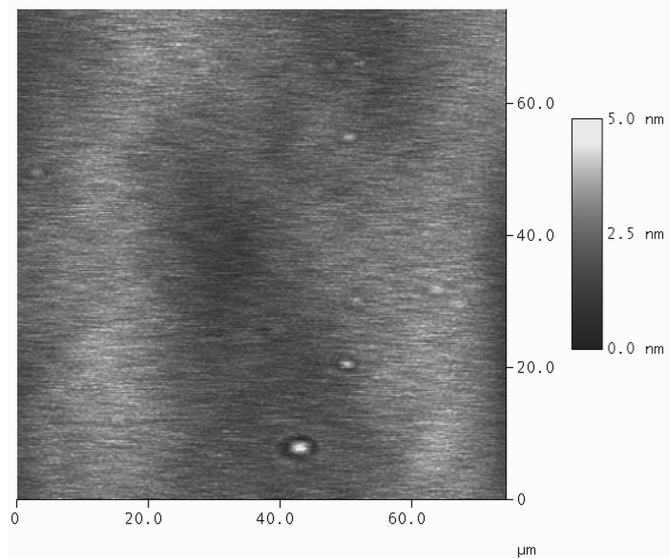


Figure 4. AFM image of the surface of the as-grown wafer.

3. DEVICE PROCESSING

Standard photolithographic techniques were used to pattern 200x200 μm test detectors on the MBE-grown wafers. Samples were dry-etched in a reactive ion etching (RIE) chamber using a mixture of Cl_2 and BCl_3 gases to a depth of 1.5 μm . Gold was evaporated onto the sample to form both the n and p-type contacts. Fig. 5 shows the IV characteristics for these test devices as a function of temperature. Excessive leakage causes the R_0A product to deviate from the ideal curve as the devices are cooled, indicating the need for a change in fabrication technique to suppress this excess leakage current.

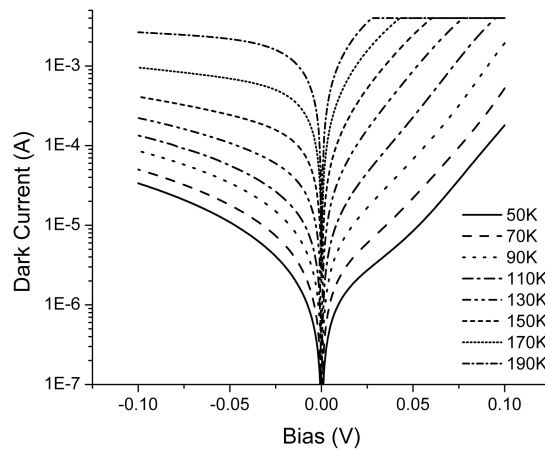


Figure 5. Dark current vs. applied bias for 200x200 μm test devices at various temperatures.

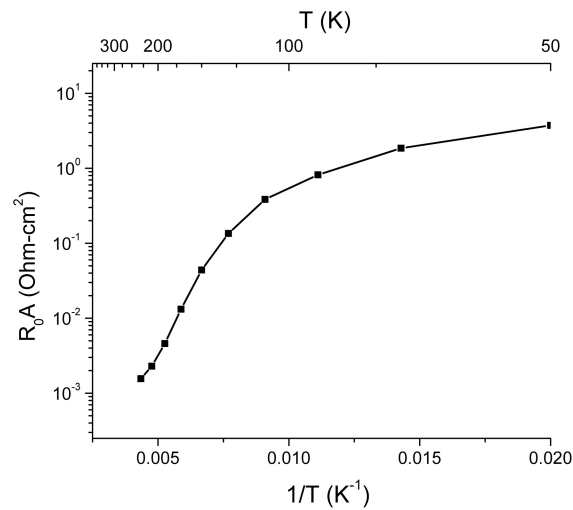


Figure 6. R_0A product as a function of temperature for the initial superlattice diodes.

To this end, several passivation techniques were applied to a second set of diodes with a slightly thicker superlattice region. All growth conditions were similar for the second set of diodes except for the addition of an extra 15 periods of undoped superlattice in the i-region. In addition to the processing steps listed above, the following post-etch treatments were applied:

- A) 30 seconds in $\text{H}_2\text{SO}_4\text{:H}_2\text{O}$ (1:40); or
- B) 2 minutes 0.05M RuCl_3 and mixed 1:1 with 0.1 M HCl.

Chemically treated samples were tested as-is and with an additional chemical vapor deposition (CVD) of SiO_2 . The CVD process was tested at two different temperatures: 250°C and 345°C.

4. RESULTS

IV curves for the 200x200 μm devices are shown in Fig. 7. Roughly a factor of 4 improvement between the best devices (RuCl_3 treatment with a high temperature oxide) and the worst devices (H_2SO_4 treatment with high temperature oxide). Unfortunately, the effects of a given dielectric deposition are not consistent within a given chemical treatment, as the order of improvement for the RuCl_3 treatment (low temperature oxide, no oxide, high temperature oxide) is different for the H_2SO_4 treatment (high temperature oxide, no oxide, low temperature oxide). There are insufficient data to determine if the variation is caused by device to device processing variations, or if the H_2SO_4 and RuCl_3 treatments actually are optimized by a low and high temperature oxide deposition, respectively. Unfortunately, in spite of the factor of four reduction in dark current, the devices are still too leaky for applications as high performance photodetectors.

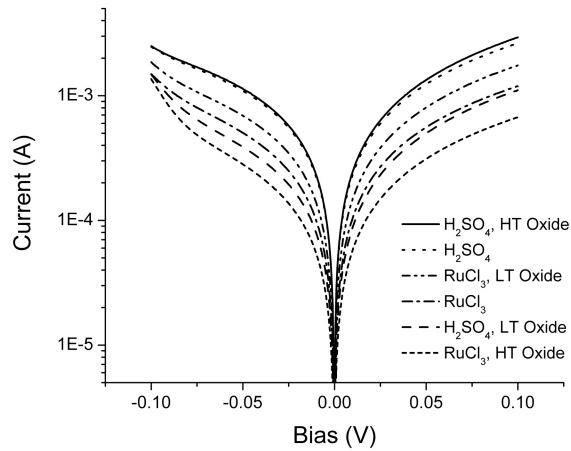


Figure 7. IV characteristics at 70K for various chemically treated diodes.

5. SUMMARY

We have tested the effects of wet chemical passivation techniques on MBE-grown GaInSb/InAs superlattice photodiodes. Although the material quality of the devices grown was excellent as evidenced by X-ray, TEM and AFM observations, the device performance is not yet good enough to allow these devices to be used in applications requiring high performance photodetectors.

6. ACKNOWLEDGEMENTS

The authors would like to thank M.Z. Tidrow and P.D. LeVan for their encouragement and guidance in developing antimony-based detectors at the Jet Propulsion Laboratory. The authors are grateful to N. Toomarian, T. N. Krabach, P. J. Grunthaler, S. Forouhar, R. Stirbl, R. Liang, and R. Cox for encouragement and support during the development and optimization of detector arrays at the Jet Propulsion Laboratory for various applications. The research described in this paper was performed by the Jet Propulsion Laboratory, California Institute of Technology, and was sponsored by the Air Force Research Laboratory and Missile Defense Agency.

REFERENCES

- 1 D.L.Smith and C.Mailhiot, J. Appl. Phys. **62**, 2545 (1987).
- 2 C.Mailhiot, and D.L.Smith, J. Vac. Sci. Technol. **A 7**, 445 (1989).
- 3 R. H. Miles and D. H. Chow, in *Long Wavelength Infrared Detectors*, edited by M. Razeghi, Chapter 7 (Gordon and Breach, Singapore, 1996); and references therein.
- 4 R. H. Miles, D. H. Chow, J. N. Schulman, and T. C. McGill, Appl. Phys. Lett. **57**, 801 (1990).
- 5 F. Fuchs, U. Weimar, W. Pletschen, J. Schmitz, E. Ahlswede, M. Walther, J. Wagner, and P. Koidl, Appl. Phys. Lett. **71**, 3251 (1997).
- 6 S.D. Gunapala and S. V. Bandara, Semiconductors and Semimetals **62**, 197 (2000).
- 7 C. H.Grein, P. M.Young, M. E. Flatté, and H. Ehrenreich, J. Appl. Phys. **78**, 7143 (1995).
- 8 F. Fuchs, U. Weimar, E. Ahlswede, W. Pletschen, J. Schmitz, and M. Walther, Proc. SPIE 3287, **14** (1998).